

Electronic Supporting information (ESI)

Mico-nano NiO-MnCo₂O₄ Heterostructure with Optimal Interfacial Electronic Environment for High Performance and Enhanced Lithium Storage Kinetics

Wei Dang ^a, Xincun Tang ^{a,*}, Wei Wang ^b, Yun Yang ^c, Xing Li ^a, Liuchun Huang ^a, Yi Zhang ^{a,*}

^a *College of Chemistry and Chemical Engineering, Central South University, Changsha 410083, P. R. China.*

^b *Key Laboratory of Hunan Province for Advanced Carbon-based Functional Materials, School of Chemistry and Chemical Engineering, Hunan Institute of Science and Technology, Yueyang, 414006, P. R. China*

^c *Key Laboratory of Ministry-of-Education for the Synthesis and Application of Organic Functional Molecules, College of Chemistry and Chemical Engineering, Hubei University, Wuhan 430062, P. R. China.*

* Corresponding author:

Email: txincun@163.com

Email: yzhangcsu@csu.edu.cn

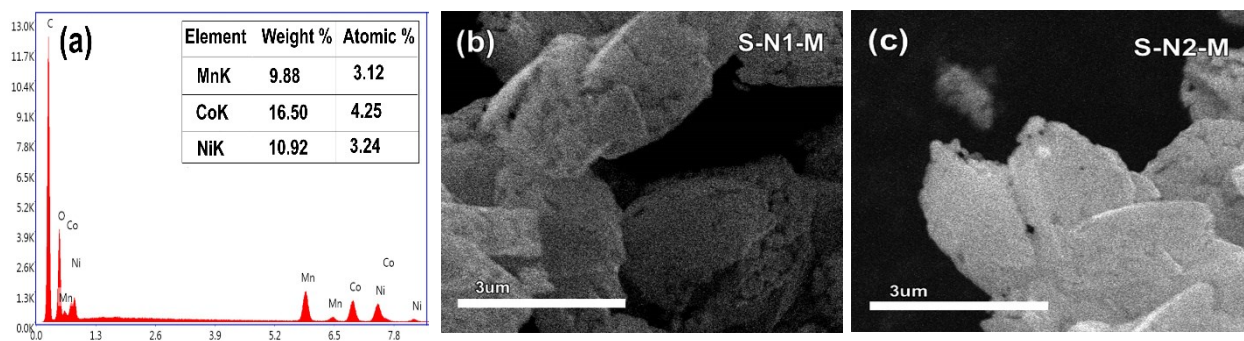


Figure S1. (a) EDS mapping of S-N-MC; (b-c) SEM images of S-N1-MC and S-N2-MC.

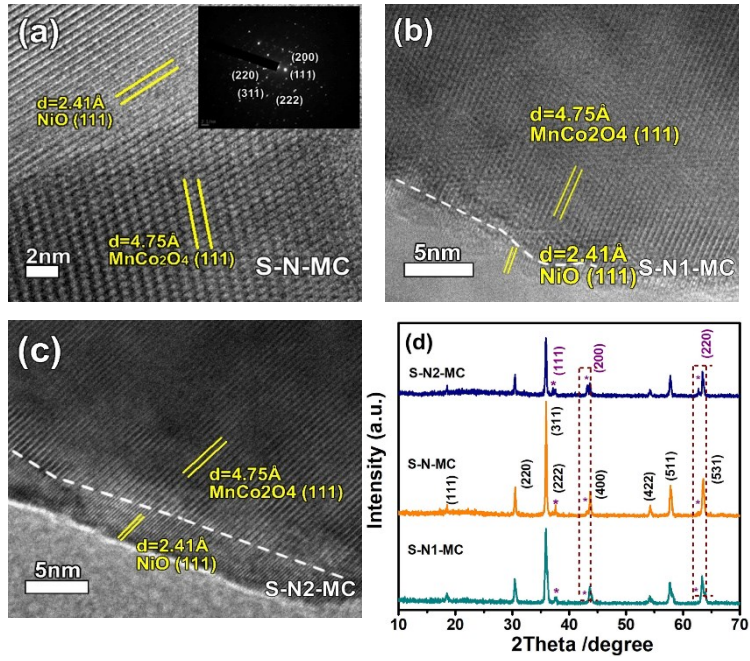


Figure S2. HRTEM images of the (a) S-N-MC heterostructure, (b) S-N1-MC, (c) S-N2-MC and (d) the corresponding XRD patterns.

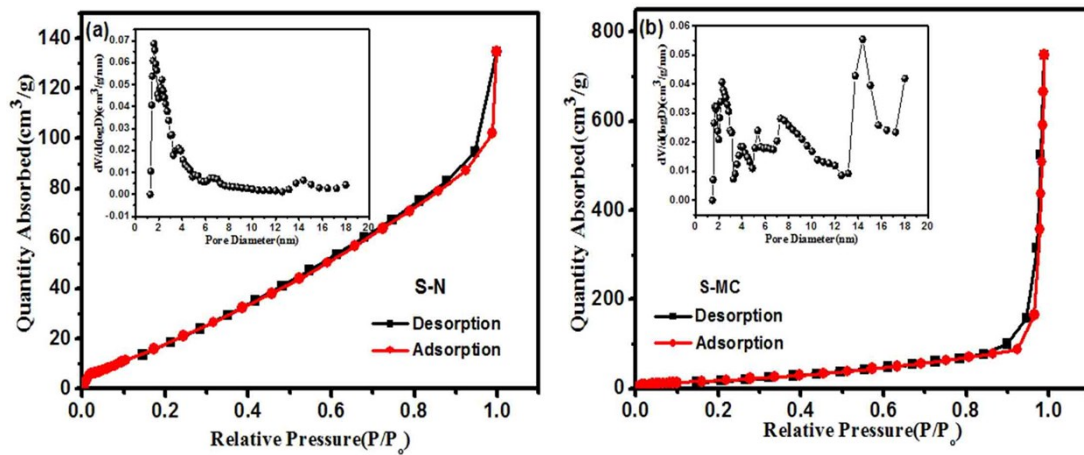


Figure S3. N₂ adsorption/desorption isotherms and the corresponding pore size distribution curves of (a) S-N and (b) S-MC.

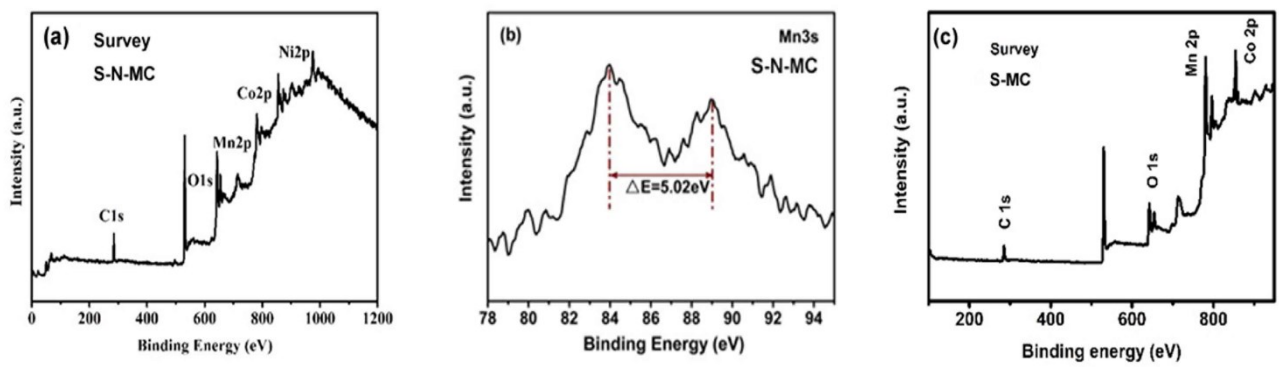


Figure S4. XPS survey spectrum of the sample (a) S-N-MC and (c) S-MC; (b) XPS patterns about Mn 3s of S-N-MC.

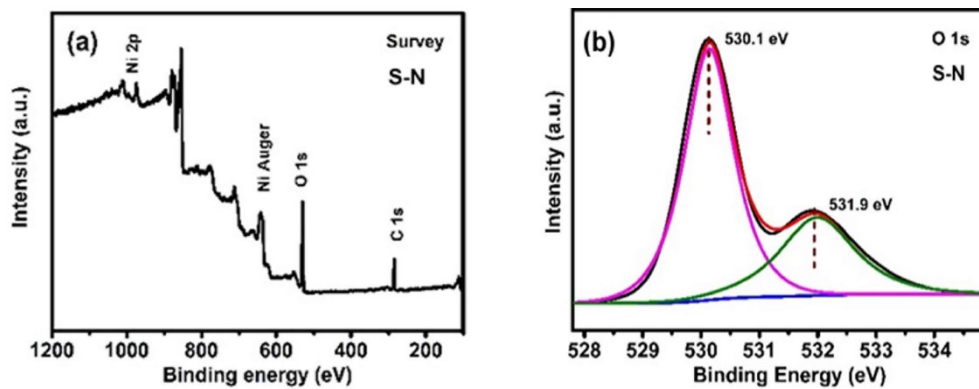


Figure S5. XPS results of S-N: (a) full scan spectra, (b) Ni 2p, (c) O 1s.

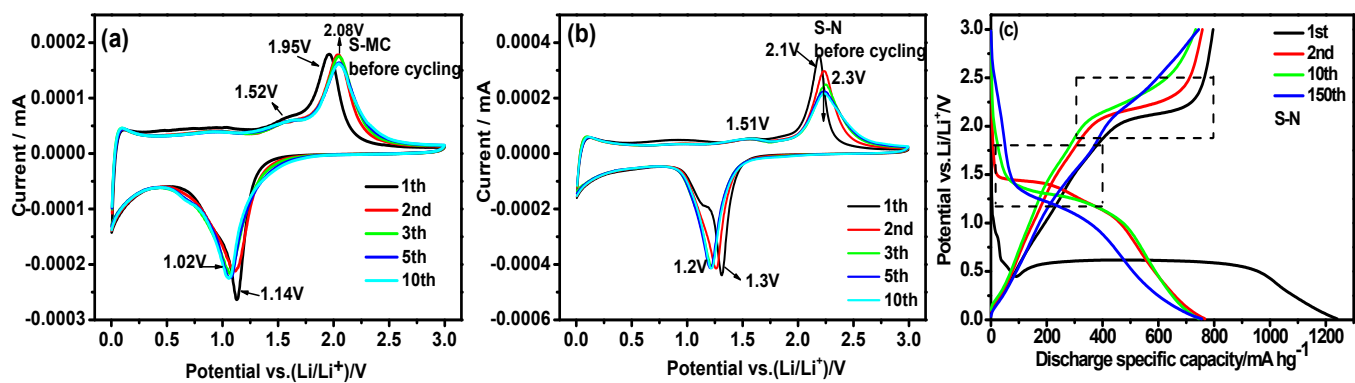


Figure S6. (a-b) CV of S-MC and S-N, (c) GDC of S-N at 500 mA h g⁻¹.

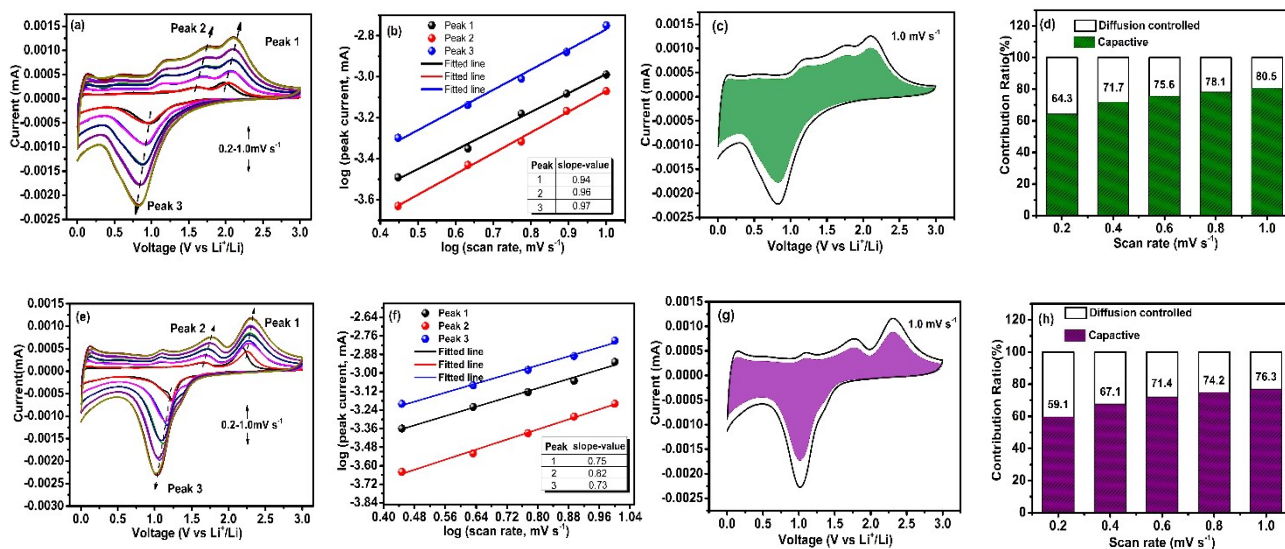


Figure S7. (a, e) CV curves at different scan rates from 0.2 to 1.0 mV s⁻¹, (b, f) Corresponding log(i) vs. log(v) plots at specific peak currents, (c, g) Shaded area of CV curve with the pseudocapacitive fraction at 1.0 mV s⁻¹, and (d, h) bar chart showing the percent of pseudocapacitive contribution at different scan rates of S-MC and (d-f) S-N.

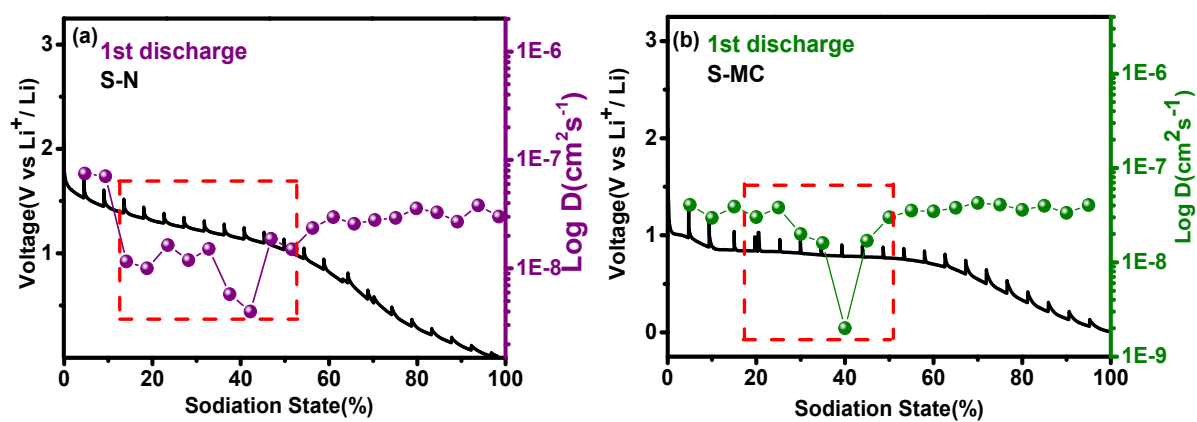


Figure S8. GITT curves and the corresponding Li^+ diffusion coefficient at different discharge/charge state of S-N and S-MC electrodes.

Table S1. Diffraction intensities of (220), (311), (511) and (531) crystal planes of S-MC and S-N-MC.

Selected crystal plane	S-MC	S-N-MC
Diffraction intensity of (220) crystal plane	975	1141
Diffraction intensity of (311) crystal plane	2841	4316
Diffraction intensity of (511) crystal plane	775	1200
Diffraction intensity of (531) crystal plane	1083	1258

Table S2. ICP-OES test on the prepared combination electrodes.

Materials	Ni/ wt%	Mn/ wt%	Co/ wt%
S-N-MC	26.2	21.3	38.1
S-N1-MC	17.3	20.9	39.3
S-N2-MC	44.7	29.6	53.2

Table S3. The crystal analysis results of S-N-MC and S-MC by Rietveld refinements.

Sample	a, b, c / Å	$\alpha, \beta, \gamma / ^\circ$	V / Å³	R_{wp} / %
S-N-MC	8.24300	90.000	568.548	2.82
S-MC	8.213728	90.000	554.142	3.85

Table S4. BET specific surface areas and pore size distributions of the samples.

Materials	BET surface area/ (m² g⁻¹)	Pore volume / (nm)
S-N	62.3	6
S-MC	63.5	33
S-N-MC	29.4	16

Table S5. Impedance fitted parameters for the electrode samples before and after cycling

Sample	S-N	S-MC	S-N-MC	S-N1-MC	S-N2-MC
Rct(ohm) bef. cycling	134.2	127.9	50.3	68.5	85.5
Rct(ohm) aft. cycling	332.8	233.2	82.1	125.1	168.7

Table S6. Reversible specific capacities of MnCo₂O₄-based sample reported before and in this work.

Morphology	Method	Current density (mA g⁻¹)	Cycle number	Remaining Density (mA h g⁻¹)	Ref.
Ni substituted MnCo ₂ O ₄ nanowires	hydrothermal method	500	200	706	[13]
NiO-MnCo ₂ O ₄ microspheres	ultrasonic nebulizer	800	300	687	[28]
multiporous MnCo ₂ O ₄	solvothermal method	400	100	610	[35]
Core-Shell Ellipsoidal MnCo₂O₄	hydrothermal method	400	70	750	[37]
MnCo ₂ O ₄ microspheres	calcination-free synthesis	900	200	320	[38]
double-shelled hollow graphene-MnCo ₂ O ₄ spheres	solvothermal method	200	100	703	[41]
Sheet or plate type morphology MnCo ₂ O ₄	molten salt method	600	70	380	[45]
NiO-MnCo₂O₄ microspheres	<u>self-assembly</u>	500 2000	500 1000	1330 719	This work